Resolving the latitudinal short-scale gravity field of Jupiter using Slepian functions

Marzia Parisi[1], Eli Galanti[2], William M. Folkner[1], Yohai Kaspi[2], Dustin R. Buccino[1]

[1]Jet Propulsion Laboratory, California Institute of Technology, Pasadena, California 91109, USA
[2]Department of Earth and Planetary Sciences, Weizmann Institute of Science, Rehovot 76100, Israel

Key Points:

- A Slepian approach is used to estimate the short-scale gravity field of Jupiter using Juno observations.
- Jupiter's gravity field determination is tailored to the geometry of the Juno orbit.
- The measured short-scale gravity field of Jupiter is explained with a thermal wind model of the zonal winds.

Corresponding author: Marzia Parisi, `marzia.parisi@jpl.nasa.gov`

Abstract

Early gravity measurements performed by the *Juno* spacecraft determined the low-degree gravitational potential of Jupiter, including the first estimate of the planet's north-south asymmetric gravity field. The retrieved information was used to conclude that the strong zonal winds visible at the cloud tops must extend down a few thousand kilometers, where they are suppressed in the deep interior. The next frontier for the Juno gravity experiment includes, among other goals, the determination of Jupiter's small-scale gravity field with high accuracy, and its relation to atmospheric circulation at shorter length scales. The geometry of the Juno closest approaches to the planet poses a challenge to this task, as they span latitudes between +4° and +29° over the course of the nominal mission. Since Doppler measurements are the most sensitive to gravity anomalies when the spacecraft is close to the body, observations of Jupiter's gravity field are mostly concentrated in the northern hemisphere, and traditional spherical harmonic functions are not orthonormal over a latitudinal subdomain. Here we define customized Slepian functions, which are orthogonal in a specific latitude range and are suitable to represent Jupiter's local surface gravity at north latitudes. We show that with the new functions, the short-scale latitudinal variability of the gravity field is resolved with high accuracy between -15° and +45° latitude. Furthermore, preliminary results show that the estimated values for the Slepian coefficients from Juno data match the predictions obtained using a thermal wind model of Jupiter's atmosphere for an optimized scale height.

1 Introduction

The gravity field of Jupiter is a mosaic of different effects of diverse origin, primarily the fast uniform rotation synchronous with the magnetic field and the differential rotation related to the strong zonal winds visible at the cloud level. Deviations from the field of a homogeneous sphere due to the former are symmetric with respect to the equatorial plane of Jupiter, much like the centrifugal acceleration. The uniform rotation response of the planet decays rapidly as a function of the harmonic degree, with the zonal coefficient of degree 10 being four orders of magnitude smaller than the degree-2 coefficient (Hubbard, 1999). On the other hand, the profile of the spherical harmonic coefficients from zonal flows is much flatter, with a difference between degrees 2 and 30 being of two orders of magnitude at most, depending on the winds' scale height (Kaspi et al., 2010). More importantly, the latitudinal profile of the Jovian winds is not north-south symmetric (Chapman, 1969), potentially giving rise to an odd gravity field if sufficiently deep. Prior to the *Juno* measurements, it was postulated that atmospheric dynamics could lead to a detectable anti-symmetric gravity field (Kaspi, 2013). One of the main scientific achievements of the Juno gravity experiment is the measurement of Jupiter's odd harmonics at low degrees, and relating their magnitude to the vertical extension of the winds within the planet's interior. The first two closest approaches of the Juno spacecraft, or perijoves, dedicated to gravity measurements (labeled as PJ3 and PJ6) were capable of answering this long standing question. The first nine zonal harmonics (J_2-J_{10}) were measured by Doppler tracking of the spacecraft (Iess et al., 2018) and the values of the odd coefficients were input to an adjoint optimization algorithm (Galanti & Kaspi, 2016) in order to determine the depth of the winds. The analysis yielded a wind depth of about 3,000 km below the visible cloud tops (Kaspi et al., 2018).

In addition to the odd gravity signal, the high-degree gravity field of Jupiter ($l > 10$) encloses valuable information about the planet's atmospheric dynamics. Beyond degree 10, the contributions to the gravity field from winds is dominant with respect to uniform rotation and the coefficients are expected to be tied to the local, short-scale structure of the jets (Kaspi et al., 2010). The geometry of the Juno science orbits renders challenging the recovery of the spherical harmonic coefficients of degree higher than 10 with the necessary accuracy. The point of closest approach between the spacecraft and the planet occurs every 53 days at altitudes between 3,500 and 8,000 km over the cloud tops.

Juno is sampling Jovian latitudes between +4° to +29° during the span of the nominal prime mission (first 33 orbits), with the perijove latitude shifting northwards by ∼1° per orbit. Doppler measurements of the spacecraft velocity are strongly affected by the gravity field of Jupiter when close to the planet, therefore the data-set available for gravity analysis is strongly skewed towards the northern hemisphere, specifically in a spherical belt comprised between latitudes -15° and +45°.

The spherical harmonic functions, used in the gravity analysis, are not orthogonal over a bounded latitudinal domain, and the high correlations between the high-degree spherical harmonic coefficients magnify the uncertainties in the parameter estimation. In this paper we explore the advantages of adopting a different function basis, Slepians, that is orthonormal over a limited latitudinal band, to represent the high-degree gravity field of Jupiter. Slepian functions are defined as linear combinations of spherical harmonics and we select the ones for which non-zero values are possible only within the chosen bounded domain (Albertella et al., 1999; Simons et al., 2009). This method was already proved useful for studying the local gravity signature of the Great Red Spot (Galanti et al., 2019), where the choice of a limited domain for the observations is dictated by the discrete nature of the mass anomaly rather than by the orbit geometry. Analogously to what was done in Kaspi et al. (2010) and Kaspi (2013) for spherical harmonics, we can expand the gravity perturbations from winds for a given scale height, using the Slepian basis. We can then assess the detectability of their signal by the Juno gravity experiment. Measurements of the higher frequency gravity field from atmospheric dynamics will complement the measurements of the global depth of the winds from low-degree odd harmonics by Kaspi et al. (2018) and potentially add information about the short-scale structure of the zonal winds.

The paper is organized as follows. In Section 2 we discuss the current Juno gravity solution halfway through its nominal mission, using the traditional spherical harmonic approach, and explain why the recovery of the high-degree coefficients is challenging. In Section 3 we introduce the Slepian functions as a linear combination of the spherical harmonic functions optimized for the Juno gravity science case. In Section 4 we expand the expected gravity signal from the winds using the Slepian functions, in order to predict the expected values for the coefficients as a function of the wind depth. In Section 5 we compare these predictions to the actual Juno measurements of the Slepian coefficients. In Section 6 we present our conclusions and discussion.

2 The gravity field of Jupiter halfway through the Juno nominal mission

In this section we present the traditional spherical harmonic approach to the estimation of Jupiter's gravity field. Our analysis combines Juno data from the first 17 science orbits, 10 of which were devoted to gravity measurements and occurred between August 2016 and December 2018. Similarly to what was done in Folkner et al. (2017), Iess et al. (2018) and, most recently, Durante et al. (2020), we start by describing the estimation process employed to retrieve the gravity coefficients characterizing the gas giant. The Juno orbit around Jupiter is very eccentric (0.98) and the spacecraft encounters the planet at close range every 53 days for a time window of a few hours. During the closest approaches, the Gravity Science instrument (Asmar et al., 2017) is extremely sensitive to perturbations in the spacecraft's radial velocity, which are related to the subtle variations in the gravity field of Jupiter.

The main observable for the Juno gravity experiment is the two-way Doppler shift on the radio carriers, enabled by the on-board radio system, which features dual-frequency links with the ground stations of NASA's Deep Space Network. In our analysis we used X- and Ka-band data (7.2–8.4 GHz and 32.5–34 GHz, respectively), received and transmitted through the on-board High Gain Antenna (HGA). Our data-set encompasses measurements collected during science orbits labeled as perijoves number 1, 3, 6, 8, 10, 11, 13, 14, 15, and 17. Most of the data were collected with the 34-m DSS 25 antenna in Goldstone, except for PJ1, which was visible from the Madrid complex (Folkner et al., 2017). Of these 10 gravity passes, 8 utilized the dual-frequency uplink and dual-frequency downlink configuration, while PJ1 and PJ13 utilized single-frequency uplink at X-band and dual-frequency downlink. In the time frame of these perijoves, the closest approaches were at latitudes between $+4°$ and $+18°$ at various Jovian longitudes (see Fig. 1) and altitudes as low as 3,500 km over the planet's upper atmosphere (Durante et al., 2020).

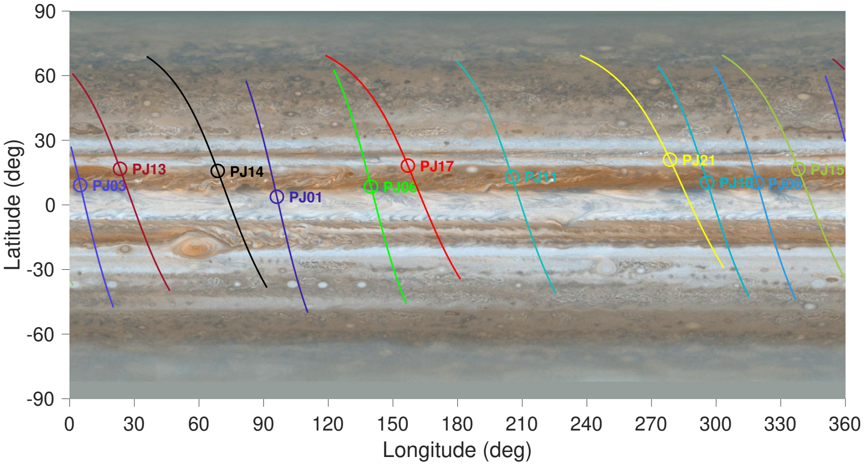

Figure 1. Juno's 10 gravity science ground tracks during the first 17 perijoves, displayed on a Jovian map as a function of the East Longitude. The closest approach latitudes (hollow circles) are contained within a limited belt in the northern hemisphere. The longitudes of the encounters are equally spaced in Jupiter System III, due to measurement requirements for the on-board Juno magnetometer. The background image is based on Cassini observations of Jupiter during the flyby in December 2000. Background image credit: NASA/JPL/Space Science Institute.

The dual-frequency link on both communication legs allows for the cancellation of up to 75% of plasma noise (50% if the uplink is single-frequency), due, among other effects, to the crossing of the Io Plasma Torus by the radio signals around perijoves (Phipps et al., 2019). Other sources of noise are from the Earth's troposphere and ionosphere. The former can be partially calibrated using empirical models of the atmosphere or measurements of the water vapor content with radiometers located at Goldstone (Asmar et al., 2005). The latter is modeled on the basis of GPS observations. The Root Mean Square (RMS) of the line-of-sight velocity residuals varies from a minimum of about 5 μms^{-1} for PJ11 to a maximum of 53 μms^{-1} for PJ1, at 60 seconds integration time, while most perijoves fall within the range 5-10 μms^{-1}.

The dynamical model used to integrate the Juno trajectory for orbit determination purposes accounts for several effects due to gravitational and non-gravitational forces acting on the spacecraft. A non-exhaustive list is: the mass of Jupiter, the Sun and the other planets (Folkner et al., 2019); Jupiter's rotational parameters (Archinal et al., 2010); Jupiter's zonal harmonic coefficients from degree 2 to 12 (Iess et al., 2018); tidal perturbations caused by the Galilean satellites up to degree 6 (Wahl et al., 2016); the mass of the Galilean satellites (Jacobson, 2018); solar pressure radiation; Jupiter's albedo and thermal emission from the planet.

Doppler data at 60 seconds integration time from the 10 gravity perijoves are combined in a multiarc square-root information filter, in order to estimate the physical parameters that characterize Jupiter's gravity. Fig. 2 shows the estimated values, and the corresponding 1-σ and 3-σ uncertainties, for the first 25 spherical harmonic coefficients which describe the axially symmetric gravity field of the planet. We label this solution as SOL1. The values are consistent with the one reported in Iess et al. (2018) and Durante et al. (2020), except for a slight difference in the value of J_2, due to different considerations used to account for the permanent tide raised by the Galilean satellites, not relevant to this study. The estimates for J_2-J_{10} (black diamonds) are well above the 1-σ and 3-σ levels (blue and green solid lines, respectively). As expected, the contribution to the even harmonics from uniform rotation decays rapidly with the harmonic degree (Hubbard, 1999), while the values of the odd harmonics, which were used by Kaspi et al. (2018) to infer the vertical extension of the winds, do not decay at higher frequencies. Beyond degree 11, the estimated values for SOL1 lie all below the 3-σ level, in some cases by as much as one order of magnitude.

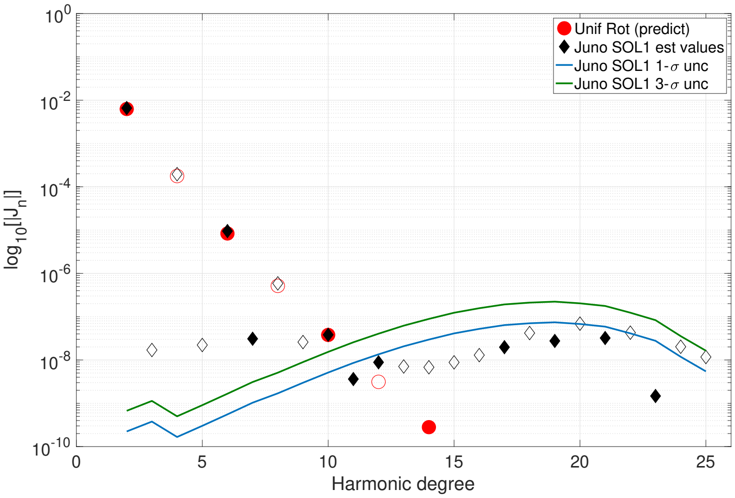

Figure 2. Spherical harmonic coefficients of Jupiter's gravity field estimated from Juno data collected during the first 17 perijoves (SOL1), as a function of the harmonic degree. The y-axis shows the normalized coefficients on a logarithmic scale. The black diamonds indicate the estimates for J_2-J_{25}. Red circles represent the predicted contributions to the gravity field with an equipotential model at rigid-body rotation. The markers are full (positive) or hollow (negative) depending on the sign. The blue and green solid lines represent the 1-σ and 3-σ formal uncertainties from Juno measurements, respectively.

A different way of looking at the recovery of Jupiter's gravity is plotting the measured surface gravity and its uncertainty as a function of latitude. Fig. 3 shows the gravity field calculated using the coefficients J_3, J_5, J_7, J_9-J_{25} and their covariance as estimated in SOL1. We omit the contribution from J_2, J_4, J_6, J_8 in order to remove the biggest contributions from uniform rotation (contributions from the winds to these four coefficients are negligible in comparison). In the latitudinal band +5° to +20°, the uncertainties on the gravity disturbances are as low as 0.1 mGal (Durante et al., 2020), whereas they reach values of several mGals between -45° to +5° and +20° to +75°. The anomalies in the polar regions are not shown in Fig. 3, since the uncertainties reach values as high as hundreds of mGal, due to the geometry of the Juno orbit. As the spacecraft continues to collect observations of the gravity field, we are bound to obtain more precise observations of the northern hemisphere, whereas observations in the southern hemisphere are still precluded.

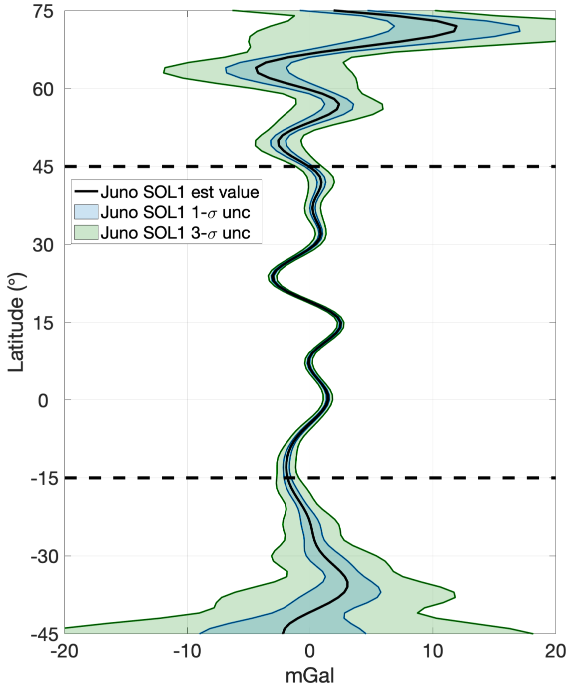

Figure 3. Jupiter's surface gravity defined with J_3, J_5, J_7, J_9-J_{25} as a function of latitude, from PJ1-PJ17 Juno gravity data analysis (SOL1). The latitudinal range is limited to -45° and +75°, which does not include the poles. The light blue and green shaded areas represent the 1-σ and 3-σ uncertainties, respectively. The gravity anomalies are known with excellent accuracy ($<$ 1 mGal) in the latitudinal band between -15° and +45°.

In conclusion, while the low-degree gravity field is accurately determined by Juno, it is challenging to estimate the high-degree, small-scale gravity anomalies of Jupiter using the traditional approach with spherical harmonic functions (SOL1). The reason is the limited range of latitudes in which the Juno perijoves occurred (+4°,+18°), where the spacecraft trajectory is subject to significant perturbations due to gravity anomalies. In a bounded latitude range, spherical harmonics are not orthogonal and the high correlations between the high-degree coefficients (J_{11}-J_{25}) result in relatively high uncertainties. The decrease in the uncertainty values after J_{20} is an artifact of the truncation of the spherical harmonic expansion at degree 25. For harmonic degrees beyond 10, the gravity signal from the winds is expected to dominate in comparison to the contribution from uniform rotation (Hubbard, 1999; Kaspi et al., 2010; Kaspi, 2013). The detection of such parameters would allow for the study of the shorter-scale dynamics and to assess whether their behavior is similar to the large-scale dynamics, as extrapolated from the analysis of the odd harmonics (Kaspi et al., 2018; 2020).

3 Slepian functions over a bounded latitudinal domain

The results shown in Section 2 advocate for the use of a different function basis, which is orthonormal in a band-limited domain, and capable of exploiting the concentrated information on Jupiter's gravity from Juno observations, while maximizing the science return. These are the Slepian functions, which have largely been used in space and Earth geodesy when the observations are not uniformly spread over the latitudinal domain (Simons & Dahlen, 2006). The Slepian approach was also successfully adopted in the case of very localized gravity signals, such as the mass anomalies caused by the Great Red Spot's turbulent flows (Galanti et al., 2019).

In this paper we follow the derivation from Albertella et al. (1999), which defined the problem of orthonormality over a spherical belt in the domain $B = \{0 \leq \lambda < 2\pi, \theta_1 \leq \theta \leq \theta_2\}$, where λ is the longitude and θ is the latitude. The optimization problem consists of maximizing the information carried by a function T over the domain B, or, analogously, minimizing the cost function (Albertella et al., 1999):

$$J\left(T\right) = \frac{\frac{1}{4\pi}\int_B T^2 d\sigma}{\frac{1}{4\pi}\int_\sigma T^2 d\sigma} = \frac{\sum_{n,m,j,k} T_{nm} T_{jk} K^B_{nmjk}}{\sum_{n,m} T^2_{nm}}, \tag{1}$$

where $d\sigma$ is the element of the surface σ of unit radius, and K^B_{nmjk} is the Gram-Schmidt matrix of the original set of functions. In our case these are known as spherical harmonics $\{Y_{nm}, |m| \leq n \leq N\}$ (Albertella et al., 1999), therefore

$$K^B_{nmjk} = \frac{1}{4\pi}\int_B Y_{nm}\left(\sigma\right) Y_{jk}\left(\sigma\right) d\sigma. \tag{2}$$

The matrix defined in Eq. (2) can be diagonalized, by finding its eigenvectors $\mathbf{a}^m_n$ and corresponding eigenvalues α^m_n. The matrix of eigenvectors A^m (whose columns are eigenvectors) is used to rotate the original basis functions Y_{nm} into the new basis functions S_{jm} (Albertella et al., 1999):

$$S_{jm}\left(\sigma\right) = \sum_{n=|m|}^{N} a^{m+}_n Y_{nm}\left(\sigma\right) \quad \{|m| \leq j \leq N\}, \tag{3}$$

where S_{jm} are the Slepian functions of degree j and order m. Every Slepian function of degree j is the linear combination of spherical harmonics of the same order m which is capable of maximizing the information over the selected latitudinal belt. As such, Slepian functions are not associated with a specific wavelength, or physical length scale like spherical harmonics (Albertella et al., 1999).

For our application to the Juno measurements of Jupiter's gravitational potential, we set -15° $< \theta <$+45°, which is the latitudinal region where the surface gravity is known with accuracies (1-σ) better than 1 mGal (Fig. 3). We define N as the maximum spherical harmonic degree used to generate the Slepian functions (Albertella et al., 1999). We chose $N = 40$ and $m = 0$, which means that each Slepian function is a linear combination of zonal spherical harmonics $Y_{2,0}$ to $Y_{40,0}$. Note that in the case the functions $Y_{n,0}$ are the zonal harmonics of degree n. Only the Slepians associated with eigenvalues larger than 0.99 are considered localized in the latitude range and are selected for our analysis. The left panels in Fig. 4 show the 9 (out of 39) normalized Slepian functions which are significant in the selected latitudinal belt and are null elsewhere, versus latitude. We renamed the functions S_{10}-S_{18}, characterized by decreasing wavelength (or increasing frequency). The spatial scale that characterizes S_{10} is comparable to the scale of zonal harmonic function $Y_{10,0}$, after being multiplied by a window function which is zero outside of the same latitudinal band. However, the frequency of the Slepian functions increases faster than the harmonics, with S_{12} that is closer to the length scale of $Y_{20,0}$.

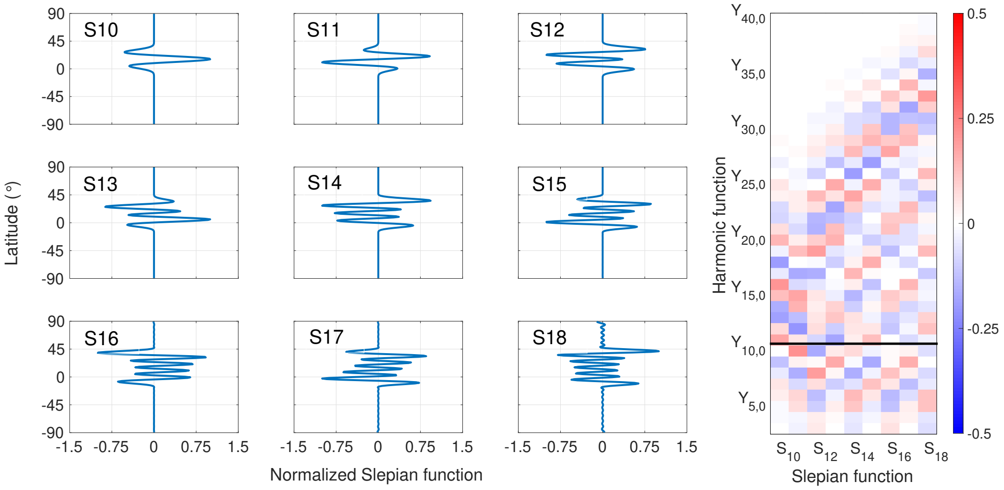

Figure 4. Left panels: the 9 Slepian functions (out of 39) defined by the transformation in Eq. (3), and which are significant only in the latitudinal band -15° $< \theta <$+45°. They are generated by combining zonal spherical harmonics from degree 2 to degree 40. We renamed the functions S_{10}-S_{18}. Right panel: correlation matrix between the 9 significant Slepians S_{10}-S_{18} (abscissa) and zonal harmonic functions $Y_{2,0}$-$Y_{40,0}$ (ordinate), over latitudes -90°, +90°. The color scale shows maximum absolute values below 0.5.

The right panel in Fig. 4 shows the theoretical correlation coefficients between the 9 selected Slepian functions (S_{10} to S_{18}) and the 39 zonal spherical harmonics used to define them. These parameters were calculated by multiplying each spherical harmonic function with each Slepian function and evaluating the integral of the product. The correlation coefficients assume values which are smaller than 0.25, indicating negligible overlap between the spherical harmonics and the Slepian functions, over the whole latitudinal domain -90°, +90°. Of particular interest are the small correlations between the low-degree spherical harmonic functions $Y_{2,0}$ to $Y_{10,0}$ and S_{10} to S_{18}, indicated on Fig. 4, for reasons that will be explained in Section 5. In reality, when reducing Juno data in the filter, the actual correlation coefficients will have different values than the theoretical ones, as they take into account several additional effects, such as the data noise level and the geometry of the orbit.

4 Projection of the short-scale gravitational signal from the winds onto the Slepian basis

Similarly to Kaspi et al. (2010) and Kaspi (2013), we calculate the density perturbations ρ' due to atmospheric dynamics visible in Fig. 1, using the thermal wind equation:

$$2\boldsymbol{\Omega}\cdot\nabla\left(\tilde{\rho}\boldsymbol{v}\right) = \nabla\rho'\times\boldsymbol{g}, \tag{4}$$

where $\boldsymbol{\Omega}$ is the planet's rigid-body rotation rate, $\tilde{\rho}$ is the hydrostatic density, $\boldsymbol{v}$ is the wind velocity and $\boldsymbol{g}$ is the gravitational acceleration. The equation holds because the Rossby number for Jupiter is small, meaning the Coriolis acceleration is balanced, to leading order, by the horizontal pressure gradient. For this calculation, we define the flow field as:

$$u\left(r,\theta\right)=u_{\text{cyl}}\left(r,\theta\right)e^{-\frac{R_J-r}{H}}, \tag{5}$$

where u is the east-west velocity component, r is the radial direction and θ is the Jovian latitude. u_{cyl} is the three-dimensional velocity profile obtained by propagating the observed wind speed at the cloud level (Tollefson et al., 2017) along the direction of the rotation axis (Kaspi et al., 2009) and R_J is Jupiter's equatorial 1-bar radius. The winds are decayed exponentially in the radial direction with the scale height H. Note that the best matches for the low-order gravity harmonics were found using more complex vertical decay functions than the exponential decay used here (Kaspi et al., 2018). However, for the purpose of this study the e-folding function is an acceptable representation of the deep dynamics of the winds.

We can derive ρ' from equation (4) using the process explained in detail in Parisi et al. (2016) and Parisi et al. (2019). The gravity signal emerging from atmospheric perturbations can be projected onto the Slepian basis, by determining the coefficients s_j of degree j related to the Slepian functions S_j using the formula:

$$s_j=\sum_{n=0}^{N}a_n^0\frac{1}{MR_J^n}\int_0^{R_J}r^{2+n}dr\int_{-1}^{1}Y_n\left(\mu\right)\rho' d\mu \tag{6}$$

where a_n^0 is the component of degree-0 (zonal) of the n^{th} eigenvector of K (eq. 2), M and R_J are Jupiter's mass and mean radius, r is the radial coordinate and μ is the cosine of the latitude.

We repeat the calculation of the coefficients s_j $(j=10,...,18)$ for different wind scale heights (H) of Eq. (5), which affects the profile of the density perturbation ρ'. In Fig. 5 we calculate the contributions from the winds to the short-scale gravity field of Jupiter in the northern hemisphere, depending on their penetration depth, from a minimum H of 100 km to a maximum of 7,000 km. The deeper the winds (increasing H), the more the mass involved in the flow and the larger the magnitude of the Slepian coefficients, similarly to the behavior of spherical harmonic coefficients shown in Kaspi et al. (2010); Kaspi (2013).

5 Juno observations of Jupiter's northern gravity field

In this section we focus on predictions for the Slepian coefficients assuming the winds are characterized by a scale height H of 1,500 km. This value is close to the best fit of the measured odd harmonics (J_3, J_5, J_7, J_9) from Juno gravity data using an adjoint optimization algorithm (Galanti & Kaspi, 2016), and assuming that the winds decay exponentially (Kaspi et al., 2020). Note that this is not the optimal profile capable of matching the observations and is used here for simplicity. In fact, the best matching profile is a more complex function which reaches down to about 3,000 km. However if one chooses to use an exponential function (as in this study), the best matching value for H is around 1,500 km. This parameter represents the e-folding scale of the function, although the winds extend deeper down for at least two scale heights.

We compare these predictions to the actual estimates for the Slepian coefficients, obtained by combining Juno Doppler data from PJ1-PJ17. In order to account for the new basis (Fig. 4, left panels), we consider a different estimation case, which we label as SOL2. The definition of the dynamical model is similar to SOL1 and the main difference is in the vector of solve-for parameters. Instead of estimating spherical harmonic coefficients J_2 to J_{25}, we estimate a combination of low-degree spherical harmonics J_2-J_{10} and the new Slepian coefficients s_{10}-s_{18}. The theoretical correlations between the parameters are below 0.25 (Fig. 4, right panel). As a consequence, although harmonic and

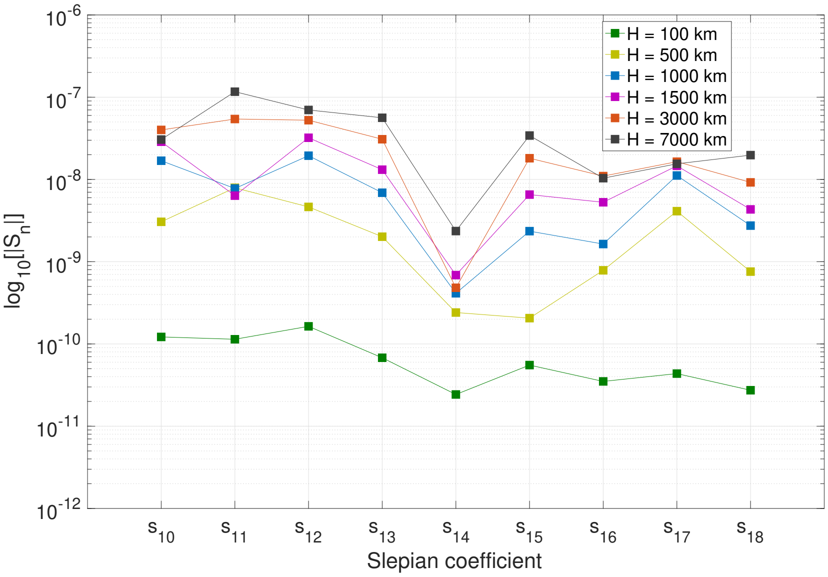

Figure 5. Predicted values for the Slepian coefficients s_{10}-s_{18} using the thermal wind model of Jupiter's atmosphere, for scale heights between 100 and 7,000 km. The signs of the coefficients are ignored in this plot, with the main focus being the amplitude of the wind signal. The y-axis shows the logarithm of the absolute value of the normalized coefficients.

Slepian functions cannot mathematically be considered orthogonal to each other, the corresponding parameters can be estimated simultaneously.

The estimated values for the combination of low-degree spherical harmonic and Slepian coefficients using Juno data from PJ1-PJ17 (SOL2) are shown in Fig. 6. The solution for the spherical harmonic coefficients J_2-J_{10} (left side) is consistent with the corresponding parameters in SOL1 (Fig. 2), except now the formal uncertainties for J_5-J_{10} are smaller, which is likely due to the reduced number of solve-for parameters and, perhaps, the abatement of some of the correlations involved. As for the Slepian coefficients (right side), the magnitude of the estimated values match that of the predictions, as well as their signs (full markers represent positive coefficients, while hollow markers are negative). Only s_{18} is characterized by opposite estimated sign to the prediction. Fig. 4 shows that the corresponding Slepian function S_{18} barely satisfies the requirement of being zero outside of the selected latitudinal belt, which might explain the discrepancy. Also, the central value for s_{18} is less than four times its formal uncertainty. The remaining estimated values for the short-scale gravity field are all above the 3-σ level (green line), sometimes by as much as one order of magnitude, with the exception of s_{14}, whose estimated value is very small and undetected. On the other hand, the predicted value for s_{14} is small compared to the other coefficients regardless of the wind scale height, as shown by Fig. 5.

The comparison between Fig. 2 and Fig. 6 highlights the advantage of using the Slepian basis, as it renders feasible the detection of the high-degree gravity field of Jupiter in the northern hemisphere. Furthermore, to first order, the short-scale circulation seems to be characterized by a depth of the same order as the large-scale flows. However, when looking at the comparison between the predicted and estimated values in more detail, the former seem to be mostly larger, indicating perhaps a shallower depth for the short-scale flows.

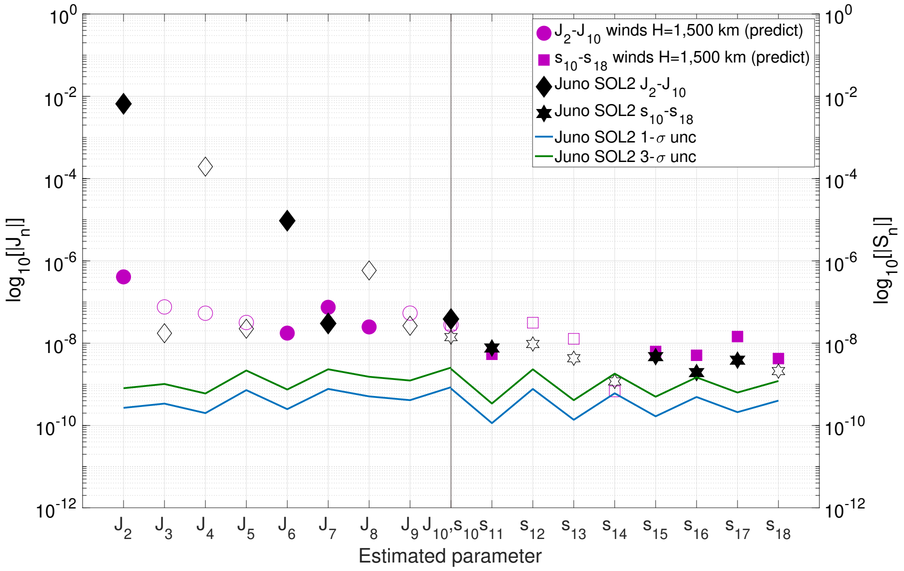

Figure 6. Solution for Jupiter's gravity field from Juno data (PJ1-PJ17), estimating a combination of low-degree spherical harmonics and Slepian functions (SOL2). The purple circles and squares indicate the coefficients from the thermal wind model of Jupiter's atmosphere with exponential decay, for a scale height of 1,500 km. The estimated values from Juno observations are represented by the black diamonds (normalized spherical harmonics) and stars (Slepians). Full markers represent positive values, while hollow markers indicate negative values. The solid blue and green lines represent the 1-σ and 3-σ uncertainty levels, respectively.

The left panel in Fig. 7 shows Jupiter's surface gravity as calculated using the estimated spherical harmonics $J_{3,5,7,9-25}$ (black line, SOL1), its 3-σ uncertainty (green shaded area, SOL1), and the surface gravity calculated from the estimated Slepian coefficients (s_{10}-s_{18}) plus low-degree spherical harmonic coefficients ($J_{3,5,7,9,10}$), represented by the dash-point black line (SOL2). The differences between the SOL1 and SOL2 surface gravity profiles are well below the 3-σ level for latitudes between -15° and +45°, which means that the set of chosen Slepian functions is appropriate to describe Jupiter's gravity within the latitudinal range. Towards the poles, the profiles tend to diverge because of the different behavior of harmonic and Slepian functions outside of the spherical belt, although in this region the surface gravity is characterized by larger uncertainties as well.

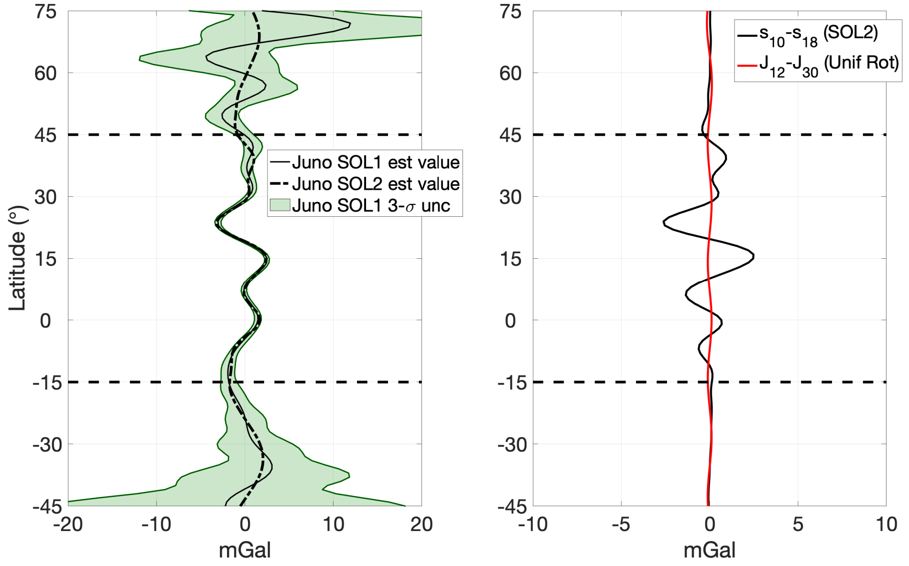

Figure 7. Left: Surface gravity from the estimated spherical harmonic coefficients $J_{3,5,7,9-25}$ (black solid line, SOL1) and from the estimated low-degree spherical harmonics $J_{3,5,7,9}$ plus Slepian coefficients s_{10}-s_{18} (black dash-point line, SOL2). The green shaded area represents the 3-σ uncertainties on the estimated surface gravity (SOL 1). Right: The black solid line shows the estimated short-scale surface gravity from Slepian coefficients s_{10}-s_{18} only (SOL2). The measured high-degree signal is compared to the predicted signal from uniform rotation beyond degree 10 (J_{12}-J_{30}), represented by the red solid line. In addition, we compare the measured signal with predictions of the surface gravity from the thermal wind model of exponentially decaying flows with H=1,500 km (purple solid line).

The right panel of Fig. 7 compares the contributions to the surface gravity from s_{10}-s_{18} alone (SOL2), to the predicted short-scale contributions from uniform rotation, which decay rapidly with the harmonic degree. Beyond degree 10, the contributions to the gravity field from uniform rotation (red solid line) are too small to explain the detected signal within the latitudinal band where the Juno observations are concentrated. Therefore, the measured high-degree gravity field is necessarily related to mass perturbations due to atmospheric dynamics.

6 Conclusion and discussion

In this paper we have shown that it is possible to detect the signature of Jupiter's short-scale zonal winds in the high-degree gravity field of the planet using Juno gravity measurements. Spherical harmonic functions are still used throughout the analysis to estimate the low-degree, global gravity field of Jupiter, while Slepian functions are used at higher degrees. The new set of functions are orthonormal and non-zero over the spherical belt defined by latitudes -15° $< \theta <$+45°, a sub-region motivated by the geometry of the Juno orbit.

The underlying assumption is that the Juno sensitivity to short-scale gravity (degree-10 and beyond) is zero outside the selected latitude band. In order to substantiate this assumption we consider the strength of the gravity signal, which decreases with the degree n like r^{n+2}, where r is the distance from the center of the planet. Since the orbit of Juno is very eccentric, the spacecraft flies over the poles (especially the south pole) at distances larger than 1.1 Jupiter radii, where the effect of J_{11} is at least 2.5 times weaker than at perijove. The comparison shown in Fig. 7 (left panel) between the surface gravity profiles from SOL1 and SOL2, demonstrate that this assumption is valid within the accuracy level of the Juno gravity measurements.

A potential limitation of the method pertains the loss of orthogonality of Slepian functions far from the reference surface. The issue has been address by Galanti et al. (2019) for the study of the Great Red Spot with two Juno perijoves, where the authors concluded that for spacecraft altitudes below 0.2 Jupiter's radii (condition satisfied when Juno flies over Jovian latitudes comprised in -15° $< \theta <$+45°), the degradation of the orthogonality of Slepian functions is negligible. Another potential limitation comes from the correlations between the different gravity coefficients involved in the estimation process. Our analysis shows that the correlations between the high-degree zonal spherical harmonics ($Y_{n,0}, n > 10$) are overall higher ($>$ 0.9 for some coefficients) than the correlations between the low-degree zonals ($Y_{n,0}, n \leq 10$) and the Slepian functions ($S_j, j = 10, ..., 18$) defined in this study (Fig. 4, right panel). As a result, lower correlations imply smaller uncertainties in the estimation of the gravity coefficients.

By combining the Juno gravity data from PJ1 to PJ17 we estimated 9 Slepian coefficients describing the short-scale gravity field of Juno, most of which are resolved to better than the 3-σ uncertainty level (except s_{14}). The estimated values were compared to the predicted gravity signal from winds with H=1,500 km, expanded in terms of Slepian functions. We found a remarkable match between the predictions and the observations, both in the central value and in sign (except for s_{18}). The accuracy associated with the Juno gravity measurements for latitudes between -15°, +45° is such that, as the winds are deeper than a few thousand kilometers, we are able to successfully detect the signature of atmospheric dynamics in the short-scale northern gravity field of Jupiter.

References

Albertella, A., Sansò, F. & Sneeuw, N. (1999). Band-limited functions on a bounded spherical domain: the Slepian problem on the sphere. *Journal of Geodesy*, 73(9), 436-447.

Archinal, B.A., A'Hearn, M.F., Bowell, E., Conrad, A., Consolmagno, G.J., Courtin, R. et al. (2010). Report of the IAU Working Group on Cartographic Coordinates and Rotational Elements: 2009. *Celestial Mechanics and Dynamical Astronomy*, 109(2), 101-135.

Asmar, S.W., Armstrong, J.W., Iess, L. & Tortora, P. (2005). Spacecraft Doppler tracking: Noise budget and accuracy achievable in precision radio science observations. *Radio Science*, 40(2). https://doi.org/10.1029/2004RS003101.

Asmar, S.W., Bolton, S.J., Buccino, D.R., Cornish, T.P., Folkner, W.M., Formaro, R. et al. (2017). The Juno Gravity Science Instrument. *Space Science Reviews*, 213, 205–218. https://doi.org/10.1007/s11214-017-0428-7.

Buccino, D.R. (2016). Juno Jupiter Gravity Science Raw Data Set V1.0, JUNO-J-RSS-1 JUGR-V1.0, NASA Planetary Data System (PDS). https://atmos.nmsu.edu/PDS/data/jnogrv_1001/

Chapman, C.R. (1969). Jupiter's Zonal Winds: Variations with Latitude. *Journal of the Atmospheric Sciences*, 26, 986-990. https://doi.org/10.1175/1520-0469(1969)026<0986:JZWVWL>2.0.CO;2

Choi, D.S. & Showman, A.P. (2011). Power spectral analysis of Jupiter's clouds and kinetic energy from Cassini. *Icarus*, 216(2), 597- 609. https://doi.org/10.1016/j.icarus.2011.10.001

Durante, D., Parisi, M., Serra, D., Zannoni, M., Notaro, V., Racioppa, P. (2020). Jupiter's gravity field halfway through the Juno mission. *Geophysical Research Letters*. e2019GL086572. https://doi.org/10.1029/2019GL086572

Folkner, W.M., Iess, L., Anderson, J.D., Asmar, S.W., Buccino, D.R., Durante, D., Feldman, M., et al. (2017). Jupiter gravity field estimated from the first two Juno orbits. *Geophysical Research Letters*, 44(10), 4694-4700. https://doi.org/10.1002/2017GL073140

Folkner, W.M., (2019). DE438 release notes. https://naif.jpl.nasa.gov/pub/naif/JUNO/kernels/spk/de438s.bsp.lbl

Galanti, E. & Kaspi Y., (2016). An adjoint-based method for the inversion of the Juno and Cassini gravity measurements into wind fields. *The Astrophysical Journal*, 820(2), 91-100. https://doi.org/10.3847/0004-637X/820/2/91

Galanti, E., Kaspi, Y., Simons, F. J., Durante, D., Parisi, M. & Bolton, S. J. & (2019). Determining the Depth of Jupiter's Great Red Spot with Juno: A Slepian Approach. *The Astronomical Journal Letters*, 874(2), https://doi.org/10.3847/2041-8213/ab1086

Hubbard, W. B. (1999). Gravitational Signature of Jupiter's Deep Zonal Flows. *Icarus*, 137(2), 357-359, https://doi.org/10.1006/icar.1998.6064

Iess, L., Folkner, W.M., Durante, D., Parisi, M., Kaspi, Y., Galanti, E., Guillot, T., et al. (2018). Measurement of Jupiter's asymmetric gravity field. *Nature*, 555, 220-222. https://doi.org/10.1038/nature25776

Jacobson., R.A. (2019). JUP310 Satellite Ephemeris File Release. https://naif.jpl.nasa.gov/pub/naif/generic_kernels/spk/satellites/jup310.cmt

Kaspi, Y., Flierl, G.R. & Showman, A.P. (2009). The deep wind structure of the giant planets: Results from an anelastic general circulation model. *Icarus*, 202(2), 525-542. https://doi.org/10.1016/j.icarus.2009.03.026

Kaspi, Y., Hubbard, W.B., Showman, A.P. & Flierl, G.R. (2010). The gravitational signature of Jupiter's internal dynamics. *Geophysical Research Letters*, Vol. 37(1), L01204. https://doi.org/10.1029/2009GL041385

Kaspi, Y. (2013). Inferring the depth of the zonal jets on Jupiter and Saturn from odd gravity harmonics. *Geophysical Research Letters*, Vol. 40(4), 676-680. https://doi.org/10.1029/2012GL053873

Kaspi, Y., Galanti, E., Hubbard, W.B., Stevenson, D.J., Bolton, S.J., Iess, L., Guillot, T., et al. (2018). Jupiter's atmospheric jet-streams extend thousands of kilometers deep. *Nature*, 555, 223-226. https://doi.org/10.1038/nature25793

Kaspi, Y., Galanti, E., Showman, A.P., Stevenson, D.J., Gulliot, T., Iess, L. & Bolton, S.J. (2020). Comparison of the deep atmospheric dynamics of Jupiter and Saturn in light of the Juno and Cassini gravity measurements. *Space Science Reviews*. Submitted.

Parisi, M., Galanti, E., Finocchiaro, S., Iess, L. & Kaspi, Y. (2016). Probing the depth of Jupiter's Great Red Spot with the Juno gravity experiment. *Icarus*, 267, 232-242. https://doi.org/10.1016/j.icarus.2015.12.011

Parisi, M., Folkner, W.M., Galanti, E., Kaspi, Y., Buccino, D.R., Oudrhiri, K. et al. (2019). A mascon approach to estimating the depth of Jupiter's Great Red

Spot with Juno gravity measurements. *Planetary and Space Science*, 104781. https://doi.org/10.1016/j.pss.2019.104781

Phipps, P.H., Withers, P., Buccino, D.R, Yang, Y.-M. (2018). Distribution of Plasma in the Io Plasma Torus as Seen by Radio Occultation During *Juno* Perijove 1. *Journal of Geophysical Research Space Physics*, 123(8), 6207-6222. https://doi.org/10.1029/2017JA025113

Phipps, P.H., Withers, P., Buccino, D.R, Yang, Y.-M., Parisi, M. (2019). Variations in the density distribution of the Io plasma torus as seen by radio occultations on Juno Perijoves 3, 6, and 8. *Journal of Geophysical Research Space Physics*, 124. https://doi.org/10.1029/2018JA026297

Schneider, T. & Liu, J. (2009). Formation of jets and equatorial superrotation on Jupiter. *Journal of the Atmospheric Sciences*, 66, 579-601. https://doi.org/10.1175/2008JAS2798.1

Simons, F.J. & Dahlen, F.A. (2006). Spherical Slepian functions and the polar gap in geodesy. *Geophysical Journal International*, 166(3), 1039-1061. https://doi.org/10.1111/j.1365-246X.2006.03065.x

Simons, F.J., Hawthorne, J.C. & Beggan C.D. (2009). Efficient analysis and representation of geophysical processes using localized spherical basis functions. *Proc. SPIE*, 7446, Wavelets XIII, 74460G (4 September 2009); https://doi.org/10.1117/12.825730

Tollefson, J., Wong, M.H., de Pater, I., Simon, A.A., Orton, G.S., Rogers, J.H., S.K. Atreya, Cosentino, R.G., Januszewski, W., Morales-Juberias, Marcus, P.S. (2017). Changes in Jupiter's zonal wind profile preceding and during the Juno mission. *Icarus*, 296, 163–178. https://doi.org/10.1016/j.icarus.2017.06.007

Wahl, S.M., Hubbard W.B. & Militzer, B. (2016). Tidal response of preliminary Jupiter model. *The Astrophysical Journal*, 831(14). https://doi:10.3847/0004-637X/831/1/14

Acknowledgments and data

We thank the Juno Interior and Atmospheric Working Groups for the useful discussions. The research described in this paper was carried out at the Jet Propulsion Laboratory, California Institute of Technology, under a contract with the National Aeronautics and Space Administration (M.P., W.M.F. and D.R.B) and at the Weizmann Institute of Science in Israel (E.G. and Y.K.). E.G. and Y.K. acknowledge support from the Israeli Space Agency, the Helen Kimel Center for Planetary Science and the Weizmann Institute of Science. The data are available through NASA's Planetary Data System at https://atmos.nmsu.edu/PDS/data/jnogrv_1001/ (Buccino et al., 2016).